Ozone-forced Southern Annular Mode during Antarctic Stratospheric Warming Events

M. Jucker[1], **R. Goyal**[1]

[1]Climate Change Research Centre and ARC Centre of Excellence for Climate Extremes, University of New South Wales, Sydney, Australia

Key Points:

- Antarctic weak vortex events can force a positive tropospheric Southern Annular Mode via radiative forcing due to high ozone concentration.
- This heating increases lower stratospheric static stability, causing a wave-driven overturning circulation to develop in the troposphere.
- This mechanism is instantaneous and opposite the slower response of negative SAM associated with ozone hole and weak vortex dynamics.

Corresponding author: Martin Jucker, `publications@martinjucker.com`

Abstract

In 2019 Southern Hemisphere spring, a strong stratospheric warming event was predicted to force the Southern Annular Mode (SAM) into a negative phase and adversely impact surface weather and Australian bushfire season for several months. Even though the negative SAM materialized towards late spring and summer, it was delayed by more than a month compared to model forecasts. Instead, the immediate surface response was a positive SAM through September to early October. Here we show that the immediate surface response was a result of circulation changes forced by anomalously high ozone concentrations which occur during Antarctic stratospheric warming events. The longer term tropospheric response was well predicted and is due to a different process acting on longer time scales. Capturing the instant coupling between dynamics and radiation in models is only possible with the inclusion of interactive ozone, which explains why most seasonal forecasting systems failed to capture it.

Plain Language Summary

In September of 2019, a rare event in the upper atmosphere was predicted to influence surface weather and worsen Australian bushfire season for several months. Even though that surface impact eventually appeared, it was delayed by more than a month compared to forecasts. Instead, the immediate surface response was opposite to what was expected through September to early October. Here we show that the immediate surface response was a result of the unusually high ozone concentrations (anomalously small ozone hole) which occur during such stratospheric events. This points to a potential for better seasonal forecasts as current forecasting systems do not include the role of stratospheric ozone.

1 Introduction

The spring 2019 stratospheric warming event (SWE) in the Southern Hemisphere (SH) was accompanied by a vertical dipole in polar cap (60-90°S) geopotential height throughout September and early October, with positive anomalies in the stratosphere and negative anomalies in the troposphere (Fig. 1a). As the event evolved in time, the stratospheric positive anomalies started to descend, and by late October the tropospheric anomalies switched signs to become positive as well. Positive polar cap geopotential height anomalies correspond to the negative phase of the Northern and Southern Annular Modes (NAM/SAM) (Gerber et al., 2010) and have long been associated with SWEs (Baldwin & Dunkerton, 2001). SWEs have attracted interest for their potential to improve seasonal forecasting in both hemispheres (Sigmond et al., 2013; Domeisen et al., 2020; Lim et al., 2019). Specifically, the negative phase of the SAM is associated with warmer and drier than usual conditions over much of Australia and South Africa, and the inverse for southern South America and New Zealand (Gillett et al., 2006).

However, the observation of a prominent and persistent positive phase of the tropospheric SAM in the spring of 2019 was surprising (Fig. 1b), and in particular its persistence (∼5 weeks) made it extraordinary: Based on reanalysis data (ERA5, see Methods), this happened only six times since 1979, with the last time more than 25 years ago in 1995. In contrast, most forecasting systems predicted a neutral SAM with a much faster transition to the negative phase during 2019 spring (Fig. 1; Rao et al., 2020). While the classic El Niño Southern Oscillation indices were neutral during 2019, there was a Central Pacific El Niño, which has been linked to the negative SAM during late spring and summer (Lim, Hendon, Butler, et al., 2021). There was also a strong positive Indian Ocean Dipole (IOD) during the spring of 2019 which can impact the wave structure in the Southern Hemisphere (Ummenhofer et al., 2009;

Lim, Hendon, Shi, et al., 2021), but its influence on the zonal mean is much smaller. In addition, the IOD was only ramping up during September and the correlation between IOD and SAM in Austral spring is weakly negative ($\sim$-0.1, Supplementary), meaning that while the IOD may be important for South Eastern Australia rainfall (Ummenhofer et al., 2009), it is not a major driver of the zonally symmetric SAM during the season of interest here. While motivated by events in 2019, we will propose a more general mechanism whereby enhanced static stability just above the tropopause induces a local anomalous circulation which then forces a positive tropospheric SAM, and that using the increased ozone concentrations associated with the SWE in a general circulation model is sufficient to produce a response similar to that observed in 2019.

2 Data and methods

2.1 Data and model

We use four different datasets for our analysis: Daily instantaneous pressure level data from ERA5 reanalysis (Hersbach et al., 2020), the sub-seasonal to seasonal (S2S) prediction dataset (Vitart et al., 2017) downloaded from the European Centre for Medium-Range Weather Forecasts (ECMWF), and two sets of simulations performed with the Community Atmosphere Model, Version 4 (CAM4; Neale et al., 2010), which is coupled to the Community Land Model Version 4 (CLM4; Oleson et al., 2010) and run with a 1.875×2.5 degree finite volume grid with 26 hybrid sigma levels. CAM4 is forced with fixed monthly climatological SSTs and sea-ice relative to 1850 and three-dimensional monthly mean ozone from ERA5. In the first set of simulations, we run a full seasonal cycle in a pre-industrial control setup, once with 2005-2015 monthly mean ozone concentrations (CTRL-S), and once with 2019 monthly mean ozone concentrations (PERT-S). The 2005-2015 period has been chosen for the CTRL ozone to avoid strong trends due to ozone hole formation. Both simulations are run for 50 years and the last 30 years are used for the analysis presented in this study. The second model setup uses the same setup as the CTRL-S simulation but we spin off 30 pairs of perpetual September simulations (fixed ozone, SST, and solar parameters) from September 1 of each year. Again, the only difference between members for each initialization is 2005-2015 mean (CTRL-P) versus 2019 ozone (PERT-P). See Fig. S3 for an illustration of the ozone setup and difference in short wave forcing. The two different setups with and without seasonal cycle are designed to separate the effects of the seasonal cycle (where the polar vortex breaks down eventually) and the ozone forcing alone. This still leaves further work to be done on effects which are included in both setups, such as the role of cloud feedbacks (Grise et al., 2013), and those which are not included in either, such as any influence of radiative effects on surface temperatures (Grise et al., 2009) (recall that SSTs are fixed to pre-industrial control climatology). Also note that by using monthly means for ozone, we miss the strong but short-lived peak in ozone concentration (i.e. the perturbation is weaker), but we gain in signal-to-noise ratio thanks to a smoother ozone field and longer periods of anomalous heating.

2.2 Methods

The main diagnostic is the Southern Annular Mode (SAM), which we define as the standardized area-weighted polar cap (south of 60S) geopotential height anomaly at each pressure level. While the standardized first principle component of zonal mean geopotential height in the southern extratropics is often used (e.g. D. W. Thompson & Wallace, 1998; Baldwin & Dunkerton, 1999; Gerber et al., 2010), the first Empirical Orthogonal Function of geopotential height is a dipole between low and high latitudes (Gerber et al., 2010) (Fig. S2). Thus using polar cap averaged geopotential height, henceforth denoted Z_{PC}, allows direct comparison between our different

datasets without having to compute principle components. Fig. 1 shows the ensemble-mean differences of PERT minus CTRL Z_{PC} with panel b) for seasonal and c) for perpetual simulations.

While these panels show the vertical Z_{PC} dipole at the center of this study, we do not rely on simple ensemble means for our analysis. Instead, for each PERT member, we define Z_{PC} anomalies as the polar cap geopotential heights minus ensemble-mean Z_{PC} from CTRL, and normalize by the cross-member Z_{CP} standard deviation at each time step and pressure level. This allows use of the same method for both CAM4 perpetual and seasonal simulations as well as ERA5. For reanalysis, the PERT members are the years 1979, 1988, 2002 and 2019 (Fig. S1, whereas the years 1981-2010 are used to compute CTRL mean and standard deviation. Finally, we composite all days across PERT members based on the single condition that $Z_{\mathrm{PC}}(500\,\mathrm{hPa}) < 0$, i.e. we do not impose a vertical dipole nor do we impose particular days of the year, as long as it occurs during September-October-November (SON).

While the S2S dataset is not part of our dynamical analysis, it is still instructive to assess the predictions of state-of-the-art seasonal forecasting systems. We did not have access to model climatologies, nor is there a control simulation, which is why we compare the differences between 30-50S and 70-90S 500 hPa geopotential height at each level and day of the year in Fig. 1. The details of how we define the SAM are of secondary importance for our analysis, as our proposed physical mechanism is ultimately based on various other dynamical variables.

We will use Eliassen-Palm fluxes (Eliassen & Palm, 1960; Andrews et al., 1983), downward control (Andrews et al., 1987; Haynes et al., 1991), the transformed Eulerian mean streamfunction (Andrews & McIntyre, 1978), and the static stability for our analysis. Eliassen-Palm fluxes are computed and scaled following (Jucker, 2021) and read

$$f_\phi = -\overline{u'v'}, \tag{1}$$

$$f_p = \left(f - \frac{1}{a\cos\phi}\frac{\partial(\bar{u}\cos\phi)}{\partial\phi}\right)\frac{\overline{v'\theta'}}{\bar{\theta}_p}, \tag{2}$$

and

$$\mathbf{F} \equiv (F_\phi, F_p) = a\cos\phi(f_\phi, f_p). \tag{3}$$

Here, u, v are the zonal and meridional wind, θ potential temperature, a Earth's radius and ϕ latitude. Overline ($\bar{\cdot}$) denotes zonal mean and prime ($'$) deviation from zonal mean. 'Downward control' refers to the findings from wave-mean flow interaction theory that the residual mean meridional overturning circulation is proportional to the vertical integral of wave activity flux above any given level (Andrews et al., 1987; Haynes et al., 1991):

$$\overline{\psi}^*(\phi, z) = \int_z^\infty \left.\frac{\rho_0 a \nabla\cdot\mathbf{F}\cos^2\phi}{\overline{m}_\phi}\right|_{\phi=\phi(z')} \mathrm{d}z', \tag{4}$$

where ψ^* is the residual streamfunction in the latitude-height plane, ρ_0 is the density of air, z height and m_ϕ the angular momentum per unit mass. $\nabla\cdot\mathbf{F}$ is Eliassen-Palm flux divergence and represents the zonal force per unit mass exerted on the zonal flow by atmospheric waves (Andrews & McIntyre, 1976). The integral is taken along constant angular momentum $\overline{m_\phi}$, but in practice is done along constant latitude as contours of angular momentum are at nearly constant latitude (Haynes et al., 1991). Static stability is represented by the Brunt-Väisälä frequency $N^2 = g\mathrm{d}\ln\theta/\mathrm{d}z$, and we will refer to 'polar cap average' as the cosine-latitude weighted zonal and meridional mean south of 60S. Finally, to assure the statistical significance of our results, we conducted two-tailed t-tests of our anomalies against the null hypothesis of zero mean, and only plot data which is significant at the 5% level in Figs. 2 and 3.

3 The role of stratospheric ozone

A warmer and weaker stratospheric polar vortex during SWEs exhibits higher geopotential heights, and limits ozone-reducing chemical reactions, which together with the increased meridional transport of ozone rich air from the tropics are responsible for anomalously high stratospheric ozone concentrations (Randel & Cobb, 1994; Plumb, 2002; de la Cámara et al., 2018; Safieddine et al., 2020, and blue dashed line in Fig. 1d). The impact on the troposphere, however, is not trivial, and we will show that the radiative impact of ozone anomalies in the lower stratosphere can explain the simultaneous negative tropospheric geopotential height anomalies (positive SAM).

Studies of tropospheric effects of stratospheric ozone anomalies have been conducted in the context of the forming and recovery of the ozone hole, and have consistently found that a positive tropospheric SAM is associated with the forming of the ozone hole and therefore a decrease in stratospheric ozone (Arblaster & Meehl, 2006; D. W. J. Thompson et al., 2011; Arblaster et al., 2011; McLandress et al., 2011), which for the case of a SWE (i.e. increased ozone) translates into a negative SAM. This is consistent with earlier work (D. W. J. Thompson et al., 2005; Lim et al., 2019) but exactly opposite the September 2019 observations. It is important to note that most studies focus on surface impacts in summer (December-February, DJF). While there is sparse evidence of inverse surface impact of ozone depletion during Austral spring compared to summer (Hurrel & Van Loon, 1994), his hasn't attracted much attention until now and the dynamical processes responsible for this behavior are largely unknown.

4 Process studies

As described above, we designed custom numerical experiments to test how stratospheric ozone anomalies may affect the tropospheric circulation, as lower stratospheric heating has been shown to have an influence on tropospheric dynamics (Simpson et al., 2009). A major difference between the model simulations and 2019 observations is that the models are not forced into producing an actual SWE, as radiative forcing from anomalous ozone is the only forcing in our experiments. While the polar vortex weakens in response to the heating, the latter is too weak to produce a 2019-like warming (Fig. S4). This approach allows us to distinguish the effects of the lower stratospheric heating associated with ozone from the dynamical heating involved in the lifecycle of an SWE. We note that to some extent the inverse experiment–i.e. dynamical heating without ozone anomalies–is represented by the S2S dataset, as those models produced an SWE but do not include interactive ozone, and failed to predict the positive SAM (Rao et al., 2020). In contrast, our model simulations show results which are similar in structure and even magnitude as seen in reanalysis, strengthening our confidence in our approach (see Figs. 1b),c) and 2).

The simulations with seasonal cycle show a vertical dipole of the correct sign starting from September, with a slowly downward propagating negative SAM (Fig. 1b). The downward propagation is what we will call the 'slow response' and corresponds to an early breakup of the polar vortex due to the additional ozone heating in PERT-S. However, recall that instead of averaging by day of year, we concentrate on instances of negative Z_{PC} anomalies and analyze the instantaneous dynamics behind it, as described in Sec. 2.2, and refer to this as the 'fast response' (Fig. 2).

During the fast response, all three datasets show the familiar vertical dipole in geopotential height anomalies with comparable tropospheric values but larger values for the stratosphere in ERA5, which is due to the additional dynamical warming which is not included in the simulations (Fig. 2 left). In latitude-pressure space, these springtime geopotential height anomalies correspond to the negative phase of the SAM in

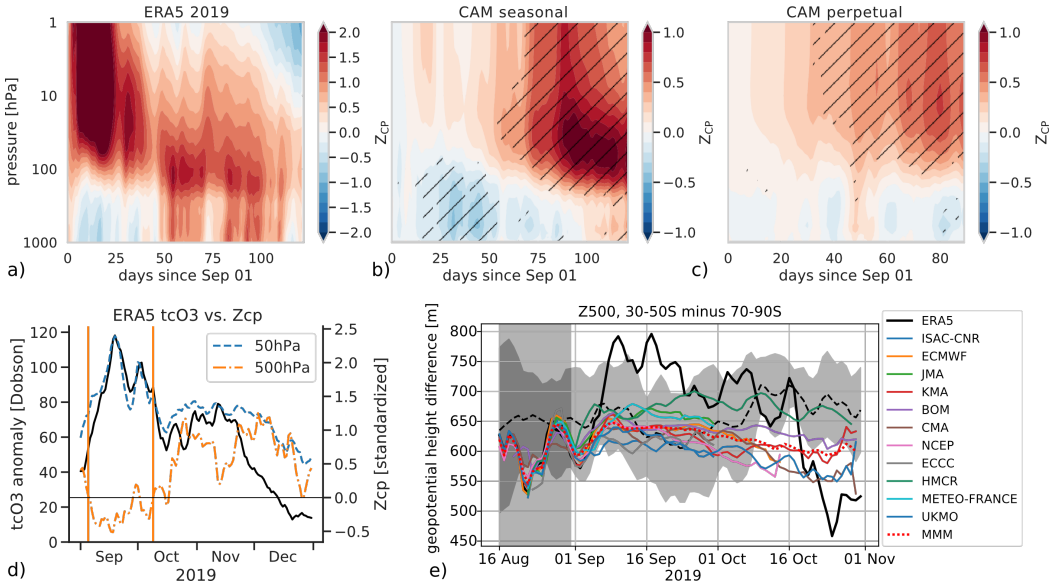

Figure 1. (a) Time-pressure plot of Z_{CP} for Spring 2019 (red/blue meaning negative/positive SAM) in ERA5. (b) 30-year average of CAM4 September-December Z_{PC} difference PERT-S minus CTRL-S. Hatching denotes regions where more than 20 years show same sign at the same day of the year. (c) Same as (b), but for PERT-P minus CTRL-P (i.e. perpetual simulations). (d) Same as (a), but for selected pressure levels. The vertical lines show the time of interest where tropospheric SAM is positive (negative Z_{PC} anomalies). (e) S2S forecasts for all model initializations between 16 and 31 August (gray box). Shown is the 500 hPa geopotential height difference between 30-50S and 70-90S (positive meaning positive SAM) for 2019 in ERA5 (black line) and S2S models (colored continuous) as well as multi-model mean (red dashed). Model data was bias corrected for same mean as ERA5 within the gray box. Black dashed line shows ERA5 2005-2015 climatology and gray shading one standard deviation during the same period.

the stratosphere and the positive phase in the troposphere (Gerber & Vallis, 2009) in both models and reanalysis (Fig. 2 center column, shading). In the troposphere, there is a clockwise anomalous circulation (panels b,e,h, solid contours) centered around 50-70°S, which explains the negative geopotential height anomalies at high latitudes and positive anomalies in midlatitudes via upwelling at high latitudes and downwelling at lower latitudes. At the same time, there is anomalous equatorward and downward Eliassen-Palm (EP) flux propagation in the upper troposphere around the same latitudes (arrows), creating positive EP flux divergence around the tropopause (right column, solid contours). The EP flux divergence explains the clockwise circulation via downward control (Eq. 4) and thus the positive SAM. Finally, the reason why EP fluxes are deflected near the tropopause instead of propagating into the stratosphere is an increase in lower stratospheric stability due to anomalous ozone heating (Fig. 2 right, shading).

This is similar to, but distinct from, a mechanism proposed earlier by Harnik and Lindzen (2001); Perlwitz and Harnik (2003, 2004) where time-lagged correlations were used to describe the reflection of waves in the upper stratosphere and a subsequent propagation back into the troposphere. These reflected waves then influence tropospheric wave structure on a time scale of about 12 days while wave-mean flow interactions influence the zonal mean tropospheric state on the long term. In this context, we note that the EP flux arrows in Fig. 2 also indicate anomalous upward propagation into the stratosphere south of 60S and anomalous downward propagation north of 60S, which might indicate reflection in the stratosphere. While the zonal wind geometry is susceptible for stratospheric wave reflection in our spring datasets in accordance with (Shaw et al., 2010), this is true for both CTRL and PERT, and the difference between the two (which is what we analyze here) does not show the time-lagged correlations described in that work. Furthermore, total EP fluxes (as opposed to anomalies) for both all waves and wave-1 are upward at all times (not shown), and Perlwitz and Harnik (2004) found that wave reflection did not influence the annular mode, which is the focus of our study. More importantly, Fig. 2 suggests that the important feature here is EP flux divergence near the tropopause, invoking downward control and therefore wave-mean flow rather than wave-wave interactions. Even so, it will be interesting to further study the relative roles of wave-wave and wave-mean flow interactions in this new context, even though separating the two might be more challenging given the important region is at the tropopause rather than high in the stratosphere, meaning any time lags due to vertical wave propagation would be very short.

At the same time as the fast response discussed above, a slower response develops which resembles the 'canonical' evolution of SWEs (Baldwin & Dunkerton, 2001; Charlton & Polvani, 2007; Jucker, 2016) (Fig. 3): After an initial fast dynamical response to stratospheric heating which takes place mostly in the troposphere, the polar vortex starts to weaken due to the dynamical heating associated with the SWE (in ERA5 only), but also the heating due to increased ozone and the seasonal cycle of solar radiation. As a result, the stability barrier in the lower stratosphere starts to erode, leading to more upward EP flux at midlatitudes, a negative EP flux divergence in the stratosphere, and weakened EP flux divergence near the tropopause. The result is a weakening of the anomalous tropospheric circulation and the associated positive SAM signal in the troposphere and the emergence of an anti-clockwise circulation in the stratosphere (Figs. 3a,b). At even longer timescales, the polar vortex starts to break down, resulting in less upward EP flux throughout the atmosphere, and downward propagation of the negative SAM signature into the troposphere (panels c,d). We note that in our model simulations with seasonal cycle, this behavior corresponds to an early breakdown of the seasonal cycle rather than a sudden warming (Fig. S4).

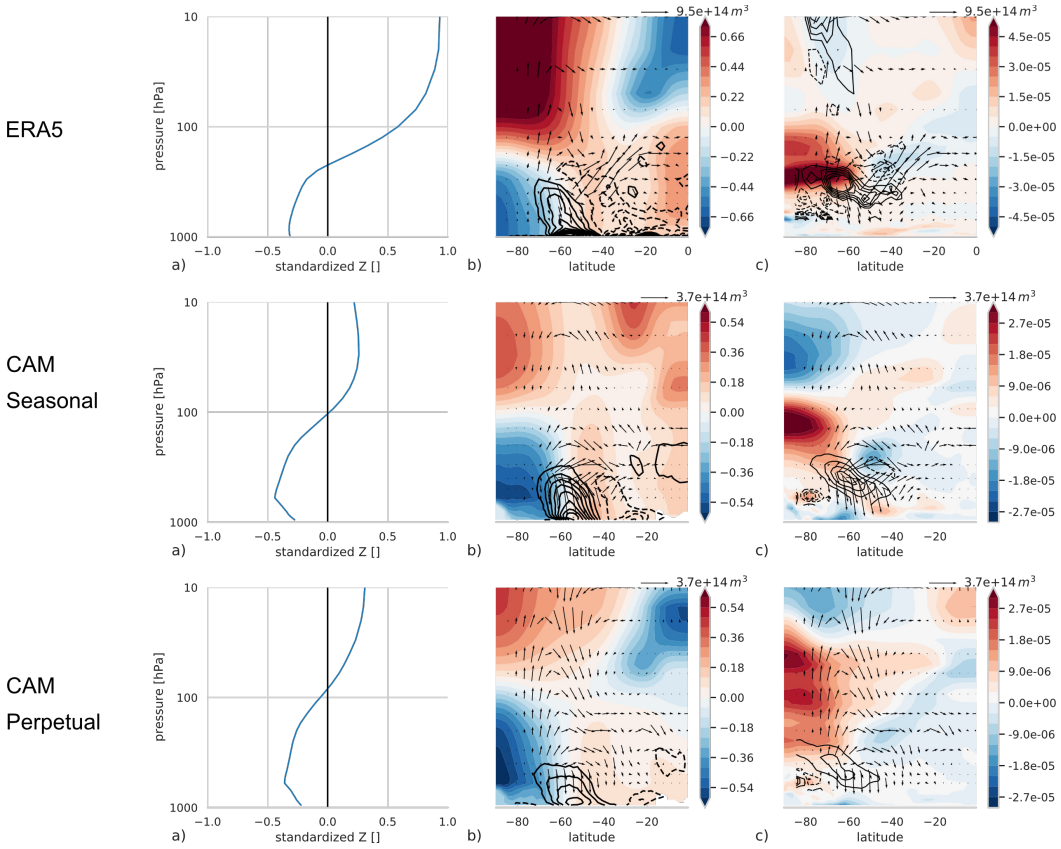

Figure 2. Composites of all days with negative Z_{PC} at 500 hPa for (top) ERA5, (middle) PERT-S minus CTRL-S, and (bottom) PERT-P minus CTRL-P. (left–a,d,g) Vertical profiles of Z_{PC}. (center–b,e,h) Geopotential height anomalies (shading), anomalous residual streamfunction (contours) and anomalous EP fluxes (arrows). (right–c,f,i) Anomalous static stability (shading), EP flux divergence (contours) and EP fluxes (arrows). Geopotential height is standardized, streamfunction is conoured in steps of 2e9 kg/s, EP flux divergence in multiples of 0.5 $\mathrm{ms}^{-1}\mathrm{d}^{-1}$. Note difference in scales between ERA5 and CAM due to the dynamical contribution of SWEs in ERA5. Only anomalies significantly different form zero are plotted according to a threshold of 5% with a two-tailed t-test, and EP fluxes plotted following Jucker (2021)

.

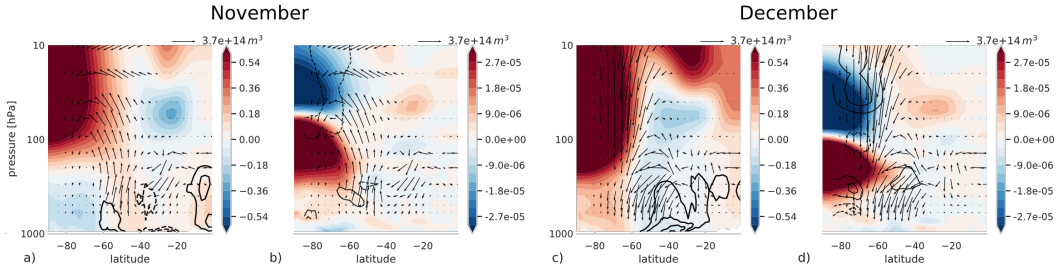

Figure 3. Longer term evolution for our simulations with seasonal cycle for (a,b) November and (c,d) December. For each month, left panels are similar to Fig. 2e) (Z_{CP}, $\overline{\psi}^*$, EP flux) and right panels to Fig. 2f) (N^2, $\nabla\mathbf{F}$ and EP flux). Rather than compositing we here show monthly means over calendar months.

5 Summary and Discussion

The emerging picture of the mechanisms can be summarized as follows (Fig. 4): As a SWE is triggered, stratospheric ozone is transported from low to high latitudes. At the same time, the stratospheric polar vortex is both warmer and less isolated, inhibiting the formation of the ozone hole (Safieddine et al., 2020). Ozone concentrations increase most in the lower stratosphere and–if the event happens in the spring when enough sunlight is available–result in localized anomalous heating close to the tropopause. The heating of the lower stratosphere in turn increases the troposphere-stratosphere contrast in static stability, causing perturbations from the troposphere to travel horizontally within the upper troposphere or be reflected downward rather than continuing vertically into the stratosphere (Chen & Robinson, 1992; Weinberger et al., 2021). Crucially, the deflection of EP fluxes creates anomalous divergence, which in turn forces a localized clockwise tropospheric circulation via downward control. That circulation includes anomalous upwelling over the polar cap and downwelling at lower latitudes, which strongly projects onto the positive phase of the Southern Annular Mode.

While we studied this mechanism in relation to weak vortex events and their associated strong ozone anomalies, it does not have to be limited to such events and can be expected to be relevant whenever lower stratospheric static stability increases. Indeed, when we select days which have negative polar cap anomalies in both the troposphere and the stratosphere from our model runs, the anomalous tropospheric circulation is still very similar to the one shown in Fig. 2, as long as there is a region of increased static stability close to the tropopause (Fig. S5). Thus, one direction for future work will be to analyze other occurrences of strong inversions above the tropopause. It is also interesting to note that while ozone concentrations do not vary as much in the Northern Hemisphere even during sudden stratospheric warmings, recent work by White et al. (2020) reported short periods of positive NAM when artificially forcing sudden warmings with an idealised model. Likewise, as discussed in this paper, the S2S forecasting systems failed to produce the positive SAM even though most predicted the strong weakening of the polar vortex. These indicate that the exact form of the heating (meridional and vertical position) matters, and presents another direction of future work.

On longer time scales, the continuous stratospheric heating due to increased ozone concentrations (and during a SWE dynamical heating) as well as the seasonal increase of insolation over high latitudes both weakens the polar vortex and decreases static stability in the upper stratosphere. With time, this allows more EP fluxes to propagate into the upper stratosphere and cause locally increased convergence, forcing an anti-clockwise circulation in the stratosphere. This signal then propagates downward similar to SWEs (Plumb & Semeniuk, 2003), and eventually forces an anomalous anti-clockwise circulation in the troposphere as well, resulting in a negative tropospheric SAM in summer. We note that while the real evolution in 2019 includes the full effect of the sudden stratospheric warming, our model simulations only include the anomalous ozone heating. Even so, our model simulations are able to reproduce the initially positive tropospheric SAM and the switch to negative SAM by early summer, albeit somewhat weaker and slower.

While many seasonal forecasting systems are forced with zonally averaged ozone concentrations, previous work reported improvements in model simulations when using fully three-dimensional ozone rather than zonally averaged ozone (Rae et al., 2019). We have conducted further model experiments with zonal mean ozone (but otherwise identical to the simulations reported here), and found that the impact of perturbed ozone was weaker, but qualitatively similar (not shown). We conclude that while zonally asymmetric ozone helps to quantitatively reproduce observed circulation anomalies, including dynamically driven perturbations (even if zonally averaged) seems to

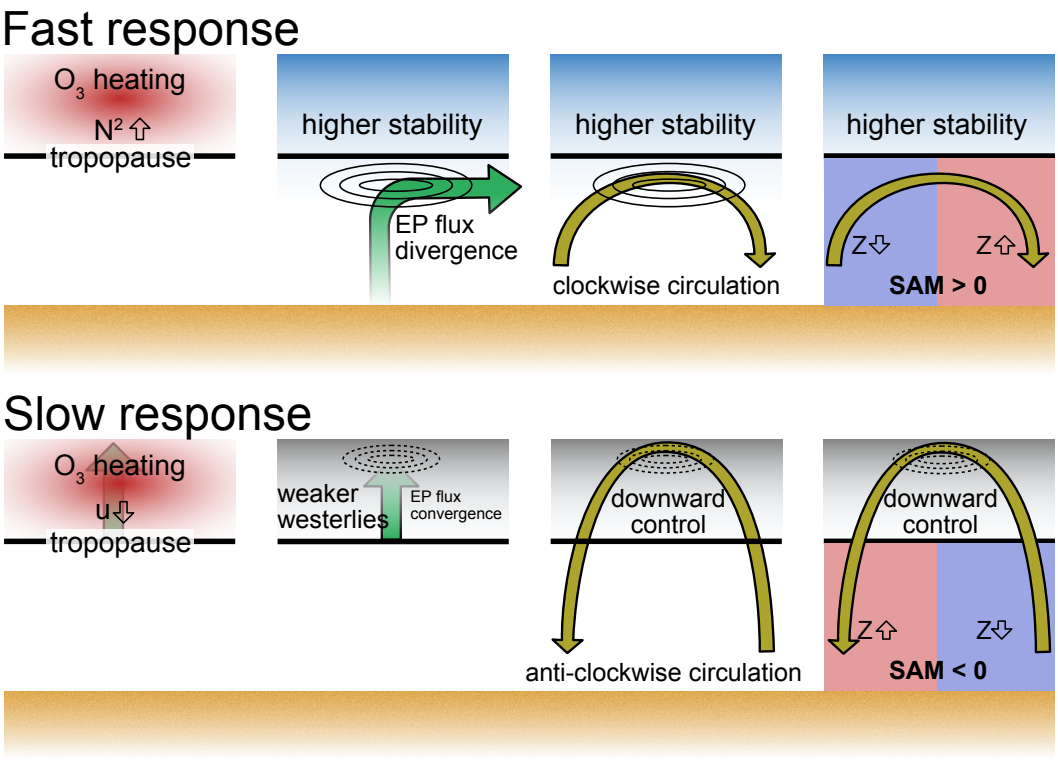

Figure 4. Schematic of the physical processes. The thick black line represents the tropopause in all panels. The fast response (top) forced the positive SAM in September/October 2019, whereas the slow response (bottom) corresponds to the more conventional 'downward propagation' of the stratospheric signal which then influences the SAM on the longer timescale (negative phase). See text for more details.

be the more important development step (Hendon et al., 2020). But in contrast to earlier studies, we find that including interactive ozone in forecasting systems should be expected to improve model performance not only during Austral summer (Rae et al., 2019; Hendon et al., 2020) but also during spring.

Acknowledgements

Both authors acknowledge support by the ARC Centre of Excellence for Climate Extremes which is supported by the Australian Research Council via grant CE170100023. MJ further acknowledges ARC grant FL150100035. This research was undertaken with the assistance of resources from the National Computational Infrastructure (NCI Australia), an NCRIS enabled capability supported by the Australian Government. We thank Amy Butler and Andrew Charlton-Perez for sharing the results from a SPARC survey of the implementation of ozone in S2S models. Model data is available at `doi.org/10.5281/zenodo.5548907`.

References

Andrews, D. G., Holton, J. R., & Leovy, C. B. (1987). *Middle Atmosphere Dynamics*. San Diego: Academic Press.

Andrews, D. G., Mahlman, J. D., & Sinclair, R. W. (1983). Eliassen-Palm Diagnostics of Wave-Mean Flow Interaction in the GFDL "SKYHI" General Circulation Model. *Journal of the Atmospheric Sciences*, *40*(12), 2768–2784. Retrieved from `http://journals.ametsoc.org/doi/abs/10.1175/1520-0469%281983%29040%3C2768%3AETWATM%3E2.0.CO%3B2` doi: 10.1175/1520-0469(1983)040⟨2768:ETWATM⟩2.0.CO;2

Andrews, D. G., & McIntyre, M. E. (1976). Planetary Waves in Horizontal and Vertical Shear: The Generalized Eliassen-Palm Relation and the Mean Zonal Acceleration. *Journal of the Atmospheric Sciences*, *33*(11), 2031–2048. doi: 10.1175/1520-0469(1976)033⟨2031:PWIHAV⟩2.0.CO;2

Andrews, D. G., & McIntyre, M. E. (1978). Generalized Eliassen-Palm and Charney-Drazin Theorems for Waves oin Axismmetric Mean Flows in Compressible Atmospheres. *Journal of Atmospheric Sciences*, *35*, 175. doi: 10.1175/1520-0469(1978)035⟨0175:gepacd⟩2.0.co;2

Arblaster, J. M., & Meehl, G. A. (2006). Contributions of External Forcings to Southern Annular Mode Trends. *Journal of Climate*, *19*(12), 2896–2905. doi: 10.1175/JCLI3774.1

Arblaster, J. M., Meehl, G. A., & Karoly, D. J. (2011). Future climate change in the Southern Hemisphere: Competing effects of ozone and greenhouse gases. *Geophysical Research Letters*, *38*(2), 1–6. doi: 10.1029/2010GL045384

Baldwin, M. P., & Dunkerton, T. J. (1999). Propagation of the Arctic Oscillation from the stratosphere to the troposphere. *Journal of Geophysical Research Atmospheres*, *104*(D24), 30937–30946. doi: 10.1029/1999JD900445

Baldwin, M. P., & Dunkerton, T. J. (2001). Stratospheric harbingers of anomalous weather regimes. *Science (New York, N.Y.)*, *294*(5542), 581–4. doi: 10.1126/science.1063315

Charlton, A. J., & Polvani, L. M. (2007). A New Look at Stratospheric Sudden Warmings. Part I: Climatology and Modeling Benchmarks. *Journal of Climate*, *20*(3), 449–469. doi: 10.1175/JCLI3996.1

Chen, P., & Robinson, W. A. (1992). Propagation of planetary waves between the troposphere and stratosphere. *Journal of Atmospheric Sciences*, *49*(24), 2533. doi: 10.1175/1520-0469(1992)049⟨2533:POPWBT⟩2.0.CO;2

de la Cámara, A., Abalos, M., Hitchcock, P., Calvo, N., & Garcia, R. R. (2018). Response of Arctic ozone to sudden stratospheric warmings. *Atmospheric Chemistry and Physics*, *18*(22), 16499–16513. doi: 10.5194/acp-18-16499-2018

Domeisen, D. I., Butler, A. H., Charlton-Perez, A. J., Ayarzagüena, B., Baldwin, M. P., Dunn-Sigouin, E., ... Taguchi, M. (2020). The Role of the Stratosphere in Subseasonal to Seasonal Prediction: 2. Predictability Arising From Stratosphere-Troposphere Coupling. *Journal of Geophysical Research: Atmospheres*, *125*(2), 1–20. doi: 10.1029/2019JD030923

Eliassen, A., & Palm, T. (1960). On the transfer of energy in stationary mountain waves. *Geofys. Publ.*, *22*(3), 1–23.

Gerber, E. P., Baldwin, M. P., Akiyoshi, H., Austin, J., Bekki, S., Braesicke, P., ... Smale, D. (2010). Stratosphere-troposphere coupling and annular mode variability in chemistry-climate models. *Journal of Geophysical Research Atmospheres*, *115*(18), 1–15. doi: 10.1029/2009JD013770

Gerber, E. P., & Vallis, G. K. (2009). On the Zonal Structure of the North Atlantic Oscillation and Annular Modes. *Journal of the Atmospheric Sciences*, *66*(2), 332–352. doi: 10.1175/2008JAS2682.1

Gillett, N. P., Kell, T. D., & Jones, P. D. (2006). Regional climate impacts of the Southern Annular Mode. *Geophysical Research Letters*, *33*(23), 1–4. doi: 10.1029/2006GL027721

Grise, K. M., Polvani, L. M., Tselioudis, G., Wu, Y., & Zelinka, M. D. (2013). The ozone hole indirect effect: Cloud-radiative anomalies accompanying the poleward shift of the eddy-driven jet in the Southern Hemisphere. *Geophysical Research Letters*, *40*(14), 3688–3692. doi: 10.1002/grl.50675

Grise, K. M., Thompson, D. W. J., & Forster, P. M. (2009). On the Role of Radiative Processes in Stratosphere–Troposphere Coupling. *Journal of Climate*, *22*(15), 4154–4161. doi: 10.1175/2009JCLI2756.1

Harnik, N., & Lindzen, R. S. (2001). The Effect of Reflecting Surfaces on the Vertical Structure and Variability of Stratospheric Planetary Waves. *Journal of the Atmospheric Sciences*, *58*(19), 2872–2894. doi: 10.1175/1520-0469(2001)058⟨2872:TEORSO⟩2.0.CO;2

Haynes, P. H., McIntyre, M. E., Shepherd, T. G., Marks, C. J., & Shine, K. P. (1991). On the "Downward Control" of Extratropical Diabatic Circulations by Eddy-Induced Mean Zonal Forces. *Journal of the Atmospheric Sciences*, *48*(4), 651–678. doi: 10.1175/1520-0469(1991)048⟨0651:OTCOED⟩2.0.CO;2

Hendon, H. H., Lim, E. P., & Abhik, S. (2020). Impact of Interannual Ozone Variations on the Downward Coupling of the 2002 Southern Hemisphere Stratospheric Warming. *Journal of Geophysical Research: Atmospheres*, *125*(16), 1–16. doi: 10.1029/2020JD032952

Hersbach, H., Bell, B., Berrisford, P., Hirahara, S., Horányi, A., Muñoz-Sabater, J., ... Thépaut, J. (2020). The ERA5 global reanalysis. *Quarterly Journal of the Royal Meteorological Society*, *146*(730), 1999–2049. doi: 10.1002/qj.3803

Hurrel, J. W., & Van Loon, H. (1994). A modulation of the atmospheric annual cycle in the Southern Hemisphere. *Tellus A*, *46*(3), 325–338. doi: 10.1034/j.1600-0870.1994.t01-1-00007.x

Jucker, M. (2016). Are Sudden Stratospheric Warmings Generic? Insights from an Idealized GCM. *Journal of the Atmospheric Sciences*, *73*(12), 5061–5080. doi: 10.1175/JAS-D-15-0353.1

Jucker, M. (2021). Scaling of Eliassen-Palm flux vectors. *Atmospheric Science Letters*, *22*(4), e1020. doi: 10.1002/asl.1020

Lim, E.-P., Hendon, H. H., Boschat, G., Hudson, D., Thompson, D. W. J., Dowdy, A. J., & Arblaster, J. M. (2019). Australian hot and dry extremes induced by weakenings of the stratospheric polar vortex. *Nature Geoscience*, *12*(11), 896–901. doi: 10.1038/s41561-019-0456-x

Lim, E.-P., Hendon, H. H., Butler, A. H., Thompson, D. W. J., Lawrence, Z., Scaife, A. A., ... Wang, G. (2021). The 2019 Southern Hemisphere stratospheric polar vortex weakening and its impacts. *Bulletin of the American Meteorological Society*, 1–50. doi: 10.1175/BAMS-D-20-0112.1

Lim, E. P., Hendon, H. H., Shi, L., de Burgh-Day, C., Hudson, D., King, A., ... Marshall, A. (2021). Tropical forcing of Australian extreme low minimum temperatures in September 2019. *Climate Dynamics*, *56*(11-12), 3625–3641. doi: 10.1007/s00382-021-05661-8

McLandress, C., Shepherd, T. G., Scinocca, J. F., Plummer, D. A., Sigmond, M., Jonsson, A. I., & Reader, M. C. (2011). Separating the dynamical effects of climate change and ozone depletion. Part II: Southern Hemisphere troposphere. *Journal of Climate*, *24*(6), 1850–1868. doi: 10.1175/2010JCLI3958.1

Neale, R. B., Richter, J. H., Conley, A. J., Park, S., Lauritzen, P. H., Gettelman, A., & Williamson, D. L. (2010). Description of the NCAR Community Atmosphere Model (CAM 4.0). *NCAR Technical Note*, *TN-485*(April), 1–196.

Oleson, K. W., Lawrence, D. M., Bonan, G. B., Flanner, M. G., Kluzek, E., Lawrence, P. J., ... Thornton, P. E. (2010). Technical Description of version 4.0 of the Community Land Model (CLM). *NCAR Technical Note*, *TN-478*(April), 1–238. doi: http://dx.doi.org/10.5065/D6FB50WZ

Perlwitz, J., & Harnik, N. (2003). Observational evidence of a stratospheric influence on the troposphere by planetary wave reflection. *Journal of Climate*, *16*(18),

435 3011–3026. doi: 10.1175/1520-0442(2003)016⟨3011:OEOASI⟩2.0.CO;2
436 Perlwitz, J., & Harnik, N. (2004). Downward coupling between the stratosphere and
437 troposphere: The relative roles of wave and zonal mean processes. *Journal of*
438 *Climate*, *17*(24), 4902–4909. doi: 10.1175/JCLI-3247.1
439 Plumb, R. A. (2002). Stratospheric Transport. *J. Meteor. Soc. Japan*, *80*(1949),
440 793–809.
441 Plumb, R. A., & Semeniuk, K. (2003). Downward migration of extratropical zonal
442 wind anomalies. *Journal of Geophysical Research*, *108*(D7), 4223. doi: 10
443 .1029/2002JD002773
444 Rae, C. D., Keeble, J., Hitchcock, P., & Pyle, J. A. (2019). Prescribing Zonally
445 Asymmetric Ozone Climatologies in Climate Models: Performance Compared
446 to a Chemistry-Climate Model. *Journal of Advances in Modeling Earth Sys-*
447 *tems*, *11*(4), 918–933. doi: 10.1029/2018MS001478
448 Randel, W. J., & Cobb, J. B. (1994). Coherent variations of monthly mean total
449 ozone and lower stratospheric temperature. *Journal of Geophysical Research*,
450 *99*(D3), 5433. doi: 10.1029/93JD03454
451 Rao, J., Garfinkel, C. I., White, I. P., & Schwartz, C. (2020). The Southern Hemi-
452 sphere Minor Sudden Stratospheric Warming in September 2019 and its
453 Predictions in S2S Models. *Journal of Geophysical Research: Atmospheres*,
454 *125*(14). doi: 10.1029/2020JD032723
455 Safieddine, S., Bouillon, M., Paracho, A. C., Jumelet, J., Tencé, F., Pazmino, A., ...
456 Clerbaux, C. (2020). Antarctic Ozone Enhancement During the 2019 Sudden
457 Stratospheric Warming Event. *Geophysical Research Letters*, *47*(14), 1–10. doi:
458 10.1029/2020GL087810
459 Shaw, T. A., Perlwitz, J., & Harnik, N. (2010). Downward Wave Coupling between
460 the Stratosphere and Troposphere: The Importance of Meridional Wave Guid-
461 ing and Comparison with Zonal-Mean Coupling. *Journal of Climate*, *23*(23),
462 6365–6381. doi: 10.1175/2010JCLI3804.1
463 Sigmond, M., Scinocca, J. F., Kharin, V. V., & Shepherd, T. G. (2013). Enhanced
464 seasonal forecast skill following stratospheric sudden warmings. *Nature Geo-*
465 *science*, *6*(2), 98–102. doi: 10.1038/ngeo1698
466 Simpson, I. R., Blackburn, M., & Haigh, J. D. (2009). The Role of Eddies in Driving
467 the Tropospheric Response to Stratospheric Heating Perturbations. *Journal of*
468 *the Atmospheric Sciences*, *66*(5), 1347–1365. doi: 10.1175/2008JAS2758.1
469 Thompson, D. W., & Wallace, J. M. (1998). The Arctic oscillation signature in the
470 wintertime geopotential height and temperature fields. *Geophysical Research*
471 *Letters*, *25*(9), 1297–1300. doi: 10.1029/98GL00950
472 Thompson, D. W. J., Baldwin, M. P., & Solomon, S. (2005). Strato-
473 sphere–Troposphere Coupling in the Southern Hemisphere. doi: 10.1175/
474 JAS-3321.1
475 Thompson, D. W. J., Solomon, S., Kushner, P. J., England, M. H., Grise, K. M.,
476 & Karoly, D. J. (2011). Signatures of the Antarctic ozone hole in Southern
477 Hemisphere surface climate change. *Nature Geoscience*, *4*(11), 741–749. doi:
478 10.1038/ngeo1296
479 Ummenhofer, C. C., England, M. H., McIntosh, P. C., Meyers, G. A., Pook, M. J.,
480 Risbey, J. S., ... Taschetto, A. S. (2009). What causes southeast Aus-
481 tralia's worst droughts? *Geophysical Research Letters*, *36*(4), L04706. doi:
482 10.1029/2008GL036801
483 Vitart, F., Ardilouze, C., Bonet, A., Brookshaw, A., Chen, M., Codorean, C., ...
484 Zhang, L. (2017). The subseasonal to seasonal (S2S) prediction project
485 database. *Bulletin of the American Meteorological Society*, *98*(1), 163–173.
486 doi: 10.1175/BAMS-D-16-0017.1
487 Weinberger, I., Garfinkel, C. I., White, I. P., & Birner, T. (2021). The Efficiency
488 of Upward Wave Propagation Near the Tropopause: importance of the form of
489 the refractive index. *Journal of the Atmospheric Sciences*, *78*(8), 2605–2617.

490 doi: 10.1175/JAS-D-20-0267.1
491 White, I., Garfinkel, C. I., Gerber, E. P., Jucker, M., Hitchcock, P., & Rao,
492 J. (2020). The generic nature of the tropospheric response to sudden
493 stratospheric warmings. *Journal of Climate*, *33*(13), 5589–5610. doi:
494 10.1175/JCLI-D-19-0697.1